S E S ' 2 0 0 5
Scientific Conference "SPACE, ECOLOGY, SAFETY" with International Participation
10–13 June 2005, Varna, Bulgaria

SOME APPLICATIONS OF THE REMOTE SENSING IN GEOLOGY BY USING OF ASTER IMAGES

Kalin Rouskov[1], Kamen Popov[1], Stanislav Stoykov[1], Ysushi Yamaguchi[2]

[1]-University of Mining and Geology "St. Ivan Rilski", Sofia 1700, Bulgaria
[2]- Department of Earth and Planetary Sciences, Nagoya University, Furo-cho, Chikusa-ku, Nagoya 464-8602, Japan
rouskov@mgu.bg, kpopov@mgu.bg, sstoykov@mgu.bg, yasushi@nagoya-u.jp

keywords: aster, remote sensing, geology

Abstract. *ASTER (The Advanced Spaceborne Thermal Emission and Reflectance Radiometer) is a research facility instrument, launched on NASA's Terra satellite in December 1999. It is sensor systems with a unique combination of wide spectral coverage and high spatial resolution. The ASTER instrument has three spectral bands in the visible and near-infrared (VNIR), six bands in the short-wave-infrared (SWIR), and five bands in the thermal infrared (TIR) regions respectively. The ASTER also has a back-looking VNIR telescope, thus, stereoscopic images are acquired at 15-m resolution. ASTER was built to serve different application areas as vegetation and ecosystem dynamics, hazard monitoring, geology and soils studies, land surface climatology, hydrology, and land cover change. The main aim of this article is to illustrate the ASTER's ability to provide an information for alteration minerals, which are valuable for mineral prospecting and exploration activities. Several band ratio composite images, highlighting the possible distributions of iron oxides and clay minerals in the area of Assarel and Medet ore deposits are given. The iron and alteration minerals spreading form two stripes, related to the faulting zones which control the development of mineral deposits and numerous ore occurrences in the studied area.*

Introduction

In its broadest sense remote sensing methods includes aerial and satellite observations of the surfaces and the atmospheres of the Earth and the other planets in our solar system also. Some of the main purposes of the remote sensing are making and updating topographic maps, weather forecasting, gathering military intelligence, etc. The focus of this article concerns some geological applications of the remote sensing for the Earth's resources investigations.

The Advanced Spaceborne Thermal Emission and Reflectance Radiometer (ASTER) is a research facility instrument, launched on NASA's Terra spacecraft in December 1999. The ASTER has 14 spectral bands in the visible and near-infrared (VNIR), the short-wave-infrared (SWIR), and in the thermal infrared (TIR) regions (ASTER Ref. Guide, 2003).

Usage of the satellite imagery has many benefits than other sources of geographic data as the aerial photography and the paper maps. For large areas satellite images are often less expensive than other sources of information. Some basic application fields of the remote sensing are listed below:

- *Geology* – prospecting and exploration of the natural resources, structural

geology, natural hazard, geological mapping, etc.

- *Hydrogeology* - exploration of the water resources, drainage analyses, etc.
- *Forestry* - determination of forest areas, recognition of the vegetation types, etc.
- *Agriculture* - agriculture area selection, agriculture production monitoring, etc.
- *Meteorology* - determination of the climate change, etc.
- *Environment* - pollution monitoring and assessment.

Specification and some applications of the ASTER images

The ASTER data is expected to contribute to many scientific areas as the geology, natural hazard monitoring, soils studies, vegetation and ecosystem dynamics, hydrology, land surface climatology, land surface and land cover change, volcano monitoring, aerosols and clouds.

The ASTER false-color and band-ratio images are very useful for the geological mapping, especially for the identification of the rock and hydrothermal alteration types (Yamaguchi et al., 1998, 2001).

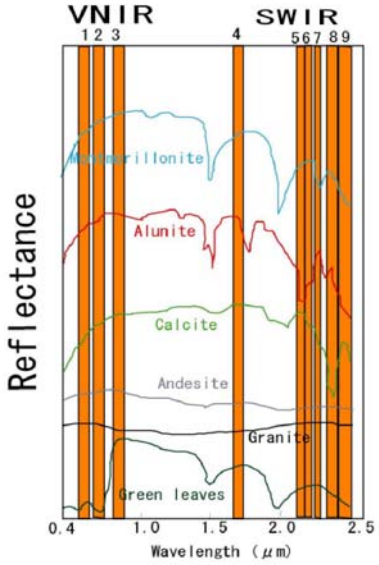

Examples for ASTER band ratio's combinations

R, G, B – 4/5, 4/6, 4/7
Alunite – red-yellow
Kaolinite – green-yellow
Calcite – blue
Montmorillonite – cyan-green
R, G, B – 2/1, 4/3, 4/5
for iron oxides and hydrothermal alteration
Alteration – blue
Iron oxides – yellow

Relative Absorption-Band Depth (RBD)
(by Crowley et al., 1989)
RBD = $(band_i + band_j)/band_k$
Ca-CO_3 absorption RBD image:
(band7+band9)/band8
Ca,Mg-CO_3 (dolomite) absorption RBD image:
(band6+band8)/band7

Fig. 1. Spectral ranges of the ASTER VNIR and SWIR bands and the reflectance spectra of some typical minerals, rocks and vegetation. The SWIR bands (5 to 9) are targeting the characteristic absorption features of these minerals.

✓ The ASTER **VNIR** data has 15m resolution, which is one of the best resolutions for multispectral data commercially available from the satellites. The VNIR can be especially useful for topographic interpretations, because of its along-track stereo coverage, as well as in assessing of the vegetation and iron-oxide minerals in surface soils and rocks.

✓ The **SWIR** data consist of 6 bands, designated as 4 to 9. The spectral bandpasses of the SWIR bands were selected for the purpose of surface mineralogical mapping. The band 4 is conformable to the spectral range where most rocks and minerals have maximum reflectivity. The bands 5 to 9 cover the Shortwave Infrared ranges where many –OH bearing and carbonate minerals have absorption features (fig. 1). Some minerals that may be of interest to the exploration geologist and which will

produce absorption features in this region are shown in table 1. Figure 1 represents some examples for the band ratios, informative for the different minerals and rock types. Band 4 is centered at the 1.65 μm, and bands 5 to 9 target the characteristic absorption features of phyllosilicate and carbonate minerals in the 2.1 to 2.4 μm region. Various approaches as principal component analysis, multiband classification and spectral indexes are useful for the geological mapping and discrimination of surface rock types in addition of band ratio images (Crosta et al., 2003; Rowan and Mars, 2002; Yamaguchi and Naito, 2003).

✓ The ASTER **TIR** data consist of 5 bands. It represents a multispectral thermal imagining data. The TIR images are useful for defining surface temperature and silica contents, although their resolution of 90 m.

✓ The ASTER VNIR subsystem includes a combination of nadir looking and backward looking bands, covering the same near infrared spectral range. These near infrared bands (assigned to bands 3N and 3B) are designed for the generation of along-track stereo-image pairs. They are used for digital elevation models (DEMs) creation and 3-dimensional stereoscopic visualization. The stereo-image pairs have a base-to-height ratio of 0.6 and intersection angle of 27.7 degrees. The DEMs are applicable in many areas as the mineral and petroleum exploration by the interpretation of geological structures on stereo-imagery, the hydrological modeling of the drainage basins, the topographic mapping and ortho-correction, etc.

Table 1. Some minerals with typical absorption features in the SWIR region.

Deposit type	Alteration minerals
Epithermal deposits	alunite, kaolinite, dickite, prophillite, illite, muscovite, jarosite, hematite
Porphyry deposits	jarosite, alunite, kaolinite, dickite, epidote, chlorite, muscovite, illite, hematite

Analysis of Band ratio images – an example for the area of Assarel and Medet ore deposits (Panagyurishte ore region)

The Assarel and Medet porphyry copper ore deposits (fig. 2) are situated within the central part of the Panagyurishte Ore Region, which is located 55–95 km east of the city of Sofia. It covers an area of about 1,500 km^2 that includes part of the central Srednogorie and Stara Planina Mountains between the towns of Pazardjik and Etropole (Popov et al., 2003a, 2003b). More than 150 ore deposits and ore occurrences and mineral indications are found in the region, which is characterized mainly by porphyry copper and epithermal massive Cu-Au deposits. Geology of the region is determined by an area of intense Late Cretaceous magmatic activity. The pre-Cretaceous basement of the Panagyurishte ore region comprises rocks of various composition and age. The main features in the geological structure are determined by the Upper Cretaceous magmatic and sedimentary rocks and the associated tectonic structures. These rocks and structures controlled the development of metallogenic processes in space and time. Younger Tertiary and Quaternary sediments cover part of the region. The post-Late Cretaceous tectonic events deformed, to differing degrees, the host rocks and structures.

The Assarel deposit is located in the central part of the Assarel volcano in an area of dense radial and concentric faulting and jointing (Strashimirov et al, 2003). The central part of the volcano is composed predominantly of lavas and brecciated lava

sheets and of dominantly andesite and latite-andesite pyroclastic rocks. The Medet deposit is located in the apical part of the Medet intrusive body of quartz-monzodiorite and granodiorite porphyry that intruded into the N-NE part of th Assarel-Medet ore field (Strashimirov et al, 2003). The basement includes Palaeozoic granites and metamorphic rocks (mainly gneisses). The most intense jointing and faulting are developed in the central and the eastern part of the intrusive body.

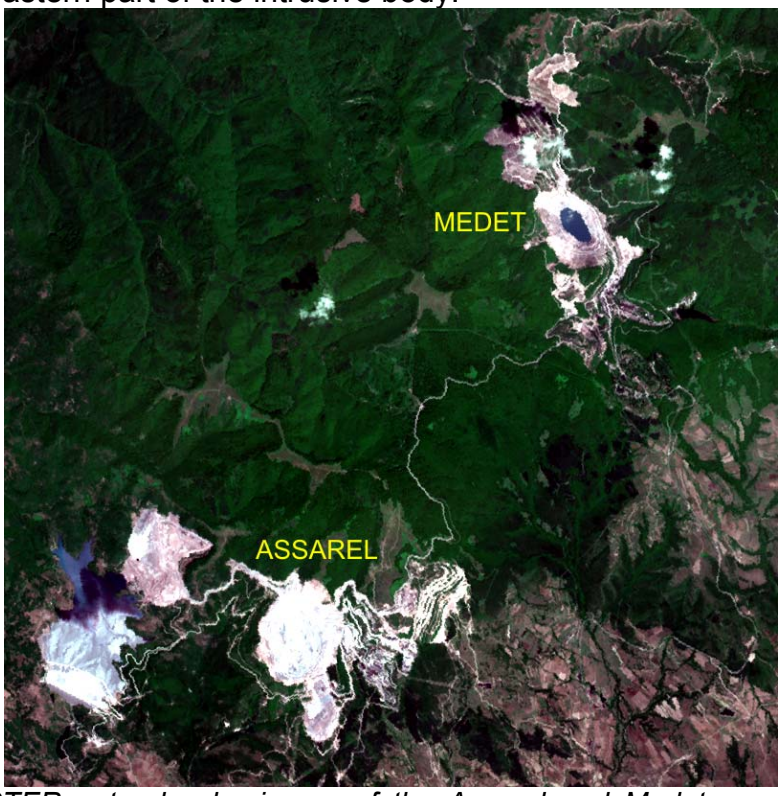

*Fig. 2. ASTER natural color image of the Assarel and Medet ore deposits (Red-B2, Green-(B1*3+B3)/4; Blue-B1).*

The part of one ASTER Level 1B scene, acquired on 16 July 2003, is processed as an example in this paper. This ASTER image was ortho-corrected to eliminate the geometric distortions. The used working projection is UTM North zone 35, WGS-1984. Some masking operations for determination of areas of interest were applied as well. The vegetation mask was extracted by usage of the NDVI index and the water mask was prepared by threshold techniques, while the cloud mask was digitized manually. The rock outcrops and soil surfaces are the target areas for analysis, so the vegetation, water and cloud masks was excluded from the study area to obtain the final “land” mask, which represent the areas of interest.

Several band-ratio images were prepared for the study area. The band rationing is a simple method for target material recognition. This procedure involves the division of two bands, where the band with high reflectance features of the given material is assigned as numerator, while the other band with high absorption features for the same material is assigned as denominator. The calculations were applied for the “land” areas of interest only, excluding the vegetated, water and cloud areas. The material’s reflectance features is determined by laboratory spectrometers usually, and they are digitally available in form of spectral libraries. The resultant grey-scale band ratio image is not a direct measurement for the material’s contents, rather it mark the areas with

highest possibilities for the presence of the given material. The combination of tree band ratio images as red-green-blue (RGB) image is very useful for the interpretation of the results. Two RGB compositions from the resultant band ratios are shown in figure 3 in comparison with false color image. The hydrothermal alterations and the alunite in particular are highlighted by the band ratio 4/5. The kaolinite and montmorillonite are highlighted by the band ratio 4/6, while 4/7 show the possible presence of calcite. Another useful band ratios are 2/1 and 4/3, which mark the presence of iron oxides.

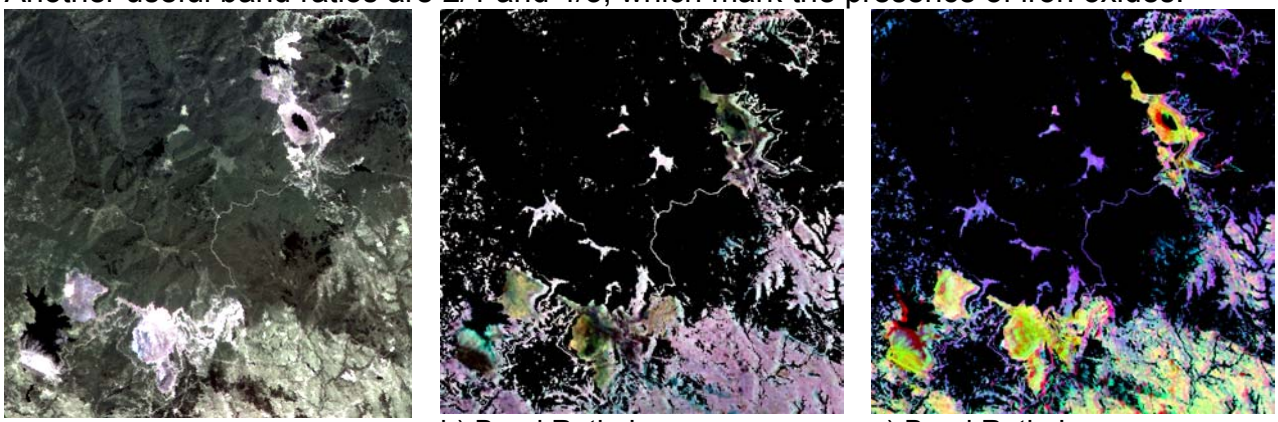

a) False Color Image
R, G, B = 5, 6, 7

b) Band Ratio Image:
R, G, B = 4/5, 4/6, 4/7

c) Band Ratio Image:
R, G, B = 2/1, 4/3, 4/5

Fig. 3. Band ratio RGB composites from ASTER shortwave infrared (SWIR) bands.

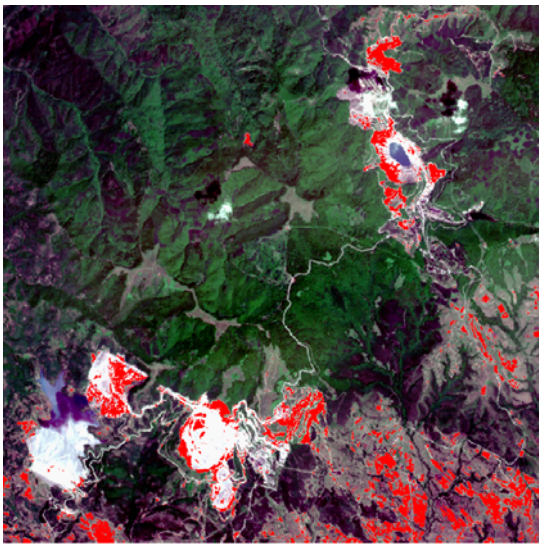

Fig. 4. ASTER natural color image overlaid by band ratio (Band 2 / Band 1). Red color represent the distribution of iron oxides.

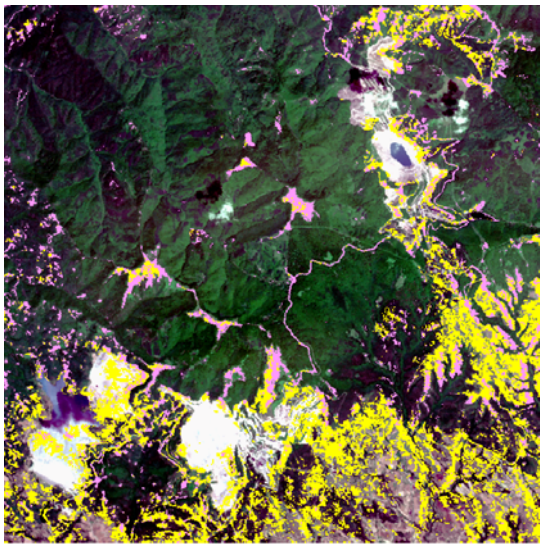

Fig. 5. ASTER natural color image overlaid by two band ratio layers for clay minerals (4/5 and 4/6). The yellow layer (ratio 4/5) is representative for the alunite and hydrothermal alterations in general. The light magenta layer (ratio 4/6) mark the distribution of the kaolinite and montmorillonite minerals.

The figure 3b represent standard RGB combination of band ratios 4/5, 4/6 and 4/7, which is useful for discrimination of the hydrothermal alterations. Here, theoretically, the possible presence of kaolinite is shown in green-yellowish colors, calcite – in bluish, alunite – in red-yellow and montmorillonite – in cyan-greenish colors.

The RGB combination of band ratios 2/1, 4/3 and 4/5, which is useful for the recognition of the iron minerals versus alterations, is shown on figure 3c. Here possible development of iron oxides are represent in yellow to reddish colors and the alteration minerals – in bluish colors.

Additional band ratio masking was applied for more precise mapping of the target materials. The statistics for the band ratio products were calculated for this purpose. For example, the possible spread of iron oxides is shown on figure 4, where the values of band ratio 2/1 greater than mean value + 2*standard deviation is mapped as red layer. The probable distribution of clay minerals is mapped on figure 5. Here the alunite and alteration minerals in general (band ratio 4/5) are shown as yellow layer, where the yellow areas correspond to 4/5 ratio values greater than mean value + 1.5*standard deviation. The light magenta layer on figure 7 highlight the presence of kaolinite and montmorillonite minerals for 4/6 ratio values greater than mean value + 2*standard deviation.

Conclusions

This paper demonstrates some powerful applications of ASTER images for geology and mineral exploration. The simple band rationing techniques can be very useful for the mapping of different rock and hydrothermal alteration types. The spatial distribution of iron oxides and clay minerals is well mapped on the ASTER image of studied area. The presence of iron minerals is typical for the highest levels of the Assarel and Medet open pits as well as for some soil areas (fig. 3, 4). Here the enrichment of iron oxides within the upper parts of the deposits is result of hydrothermal alteration processes, while the iron enrichment of soils is due to the weathering mainly. The clay minerals are spread around the deposits and within some soil areas as their distributions are well mapped on figure 3b and 3c. The clay mineral's spreading mapped on figure 3 represent the natural clay enrichment of the rocks and soils, but the hydrothermal alteration minerals are not well mapped on this figure. Additional sophisticated image classification can be applied for mineral discrimination. However the precision of the results is limited by the spectral resolution of the imagery as well as by the material mixing within the individual pixels.

The spatial distribution of iron and alteration minerals clearly forms two stripes (fig. 4, 5). The firs stripe is situated along the NW-SE oriented Medet fault, which controls the development of the Medet intrusive and the Medet ore deposit. The second stripe possesses longitudinal direction and mark the area of intersections of the longitudinal and diagonal faults in the Assarel deposit area. The Assarel and Orlovo Gnezdo deposits as well as numerous ore occurrences are developed in this area. The iron oxides spreading mark the weathering products of pyrite and iron minerals mainly (band ratio 2/1 on fig. 4). The band ratio 4/5 highlights the presence of alunite and the products of the superimposed hydrothermal and supergene processes (fig. 5). The kaolinite and montmorilonite are typical for granite rocks and the resulting soils, so their distribution is genetically determined in the eastern and southern areas, where the Paleozoic granite is widespread.

The demonstrated processing methods are applicable for digital rock and alteration type mapping, which is one of the main targets for the prospecting and research of mineral deposits.

Acknowledgments

The authors like to express their appreciations to the Japan International Cooperation Agency (JICA) for the grant in development of the Remote Sensing and GIS Laboratory at the University of Mining and Geology “St. Ivan Rilski”, Sofia. The valuable assistance was received by the Land Processes Distributed Active Archive Center (LP DAAC) at the U.S. Geological Survey, which provide the ASTER images to our RS&GIS laboratory. This investigation is supported also by the National Science Fund of Bulgaria by project H3-1412.

References

ASTER Reference Guide Version 1.0. 2003. Earth Remote Sensing Data Analysis Center.

Crosta, A., De Souza Filho, C., Azevedo, F., Brodie, C., 2003. Targeting key alteration minerals in epithermal deposits in Patagonia, Argentina, using ASTER imagery and principal component analysis. INT. J. REMOTE SENSING, VOL. 24, NO. 21, 4233–4240.

Crowley, J.K., Brickey, D.W, and Rowan, L.C. 1989. Airborne imaging spectrometer data of the Ruby Mountains, Montana: mineral discrimination using relative absorption band-depth images. Remote Sensing of Environment, 29, 121-134.

Popov, P., S. Strashimirov, K. Popov, R. Petrunov, M. Kanazirski, D. Tsonev. 2003a. Main Features in Geology and Metallogeny of the Panagyurishte Ore Region. An. Univ. Min. Geol., vol. 46, part. I, 119-125.

Popov, P., S. Strashimirov, K. Popov. 2003b. Geology and metallogeny of the Srednogorie zone and Panagyurishte ore region. In: Cretaceous Porphyry-Epithermal Systems of the Srednogorie Zone, Bulgaria. SEG Guidebook series, vol. 36, 7-26.

Rowan, L., Mars, J., 2002. Lithologic mapping in the Mountain Pass, California area using Advanced Spaceborne Thermal Emission and Reflection Radiometer (ASTER) data. Remote Sensing of Environment 84, 350–366.

Strashimirov, S., K. Bogdanov, K. Popov, R. Kehayov. 2003. Porphyry systems of the Panagyurishte ore region. In: Cretaceous Porphyry-Epithermal Systems of the Srednogorie Zone, Bulgaria. SEG Guidebook series, vol. 36, 47-78.

Yamaguchi, Y., Naito, C., 2003. Spectral indices for lithologic discrimination and mapping by using the ASTER SWIR bands. INT. J. REMOTE SENSING, vol. 24, 4311 – 4323.

Yamaguchi, Y., Kahle, A. B., Tsu, H., Kawakami, T., and Pniel, M., 1998. Overview of Advanced Spaceborne Thermal Emission and Reflection Radiometer (ASTER). IEEE Transactions on Geoscience and Remote Sensing, 36, 1062–1071.

Yamaguchi, Y., Fujisada, H., Tsu, H., Sato, I., Watanabe, H., Kato, M., Kudoh, M., Kahle, A.B., Pniel, M., 2001. ASTER early image evaluation. Adv. Space Res. Vol. 28, No. 1, 69-76.